Molecular Crystals and Liquid Crystals
Publication details, including instructions for authors and subscription information:
http://www.tandfonline.com/loi/gmcl16

An X-ray Diffraction Study of Three Mesophases Showing Smectic A Morphology

W. R. Krigbaum [a] , J. C. Poirier [a] & M. J. Costello [a b]
[a] Gross Chemical Laboratory, Duke University, Durham, N.C., 27706
[b] Dept. of Anatomy, Duke University Medieal Center, Durham, N.C., 27710
Version of record first published: 21 Mar 2007.

To cite this article: W. R. Krigbaum , J. C. Poirier & M. J. Costello (1973): An X-ray Diffraction Study of Three Mesophases Showing Smectic A Morphology, Molecular Crystals and Liquid Crystals, 20:2, 133-163

To link to this article: http://dx.doi.org/10.1080/15421407308083308

Molecular Crystals and Liquid Crystals. 1973. Vol. 20, pp. 133–163

Printed in Great Britain

An X-ray Diffraction Study of Three Mesophases Showing Smectic A Morphology†

W. R. KRIGBAUM, J. C. POIRIER and M. J. COSTELLO‡

Gross Chemical Laboratory
Duke University
Durham, N.C. 27706

Received February 9, 1972; *in revised form September* 29, 1972

Abstract—A diffraction study is reported of highly oriented samples of the smectic *A* mesophases of bis(*p*-*n*-hexyloxyphenyl)mercury (BHPM), ethyl *p*-azoxybenzoate (EPAB), and thallium stearate (TLST). Data were collected from stepped drops for the latter two compounds. Distortions of the first kind make a significant contribution to the lattice imperfections in these mesophases, while distortions of the second kind are less important than anticipated for such fluid materials. After correction for distortions, the structure amplitudes of the sharp meridional reflections decrease monotonically with order. The rate of decrease followed the order BHPM > EPAB > TLST, hence the numbers of reflections which could be collected were 2, 3 and 6, respectively. Least-squares refinement of one to three parameters for proposed model structures was used to best fit the observed structure amplitudes. No suitable representation could be obtained using a two parameter model for the smectic phase of BHPM, but those of the other two materials were well satisfied by a three parameter model. This involves a centro-symmetric dimer motif having the two molecules displaced 6 to 7 Å along their long axes, and the dimer tilted with respect to the normal to the smectic layers so that the ends of the molecules overlap the smectic planes by less than 1 Å. This structure contradicts the commonly held view concerning the distinction between smectic *A* and *C* phases, according to which the molecules are perpendicular to the layers in the former and tilted in the latter.

1. Introduction

Certain crystalline solids do not form the expected isotropic liquid upon melting, but instead produce a fluid phase which retains some degree of order. These liquid crystalline phases (or meso-

† This work, supported in part by Grant from the National Science Foundation, was submitted by M.J.C. in partial fulfillment of the requirements for the degree of Doctor of Philosophy, 1971.

‡ Present address: Dept. of Anatomy, Duke University Medical Center, Durham, N.C. 27710.

phases) may be divided into two major categories, nematic and smectic, where the cholesteric mesophase is regarded as a twisted nematic phase. In addition to such *thermotropic* mesophases formed by heating, there exist *lyotropic* mesophases which result upon the addition of solvent. Mesophases have been the subject of recent and extensive reviews.[1]

Large differences in the macroscopic physical properties, especially the optical behavior, underlie the common operational method of distinguishing nematic from smectic phases by examination under a polarizing microscope using crossed polarizers. With specially prepared supporting surfaces, or in an orienting magnetic field, or by careful growth of the mesophase from another thermodynamic phase, the entire mesophase sample may be obtained in an optically uniform condition indicative of a single liquid crystal. Use of such samples facilitates the interpretation of both optical data and data from methods sensitive to the organization at the molecular level, such as X-ray diffraction. This latter method has been used in a number of rather different ways. As applied to nematic phases, molecular orientation distribution functions have been derived from quantitative intensity measurements,[2] while recently photographic diffraction patterns have been proposed[3–5] as a basis for subdividing nematic phases into three polymorphic types. Structural studies based on the diffraction of single crystals and single liquid crystals appear to be a promising route to our ultimate goal, which is understanding the changes in molecular organization as the crystal is heated and passes through one or more mesophases to the isotropic liquid. Detailed information concerning the molecular structure can only be obtained from study of the crystalline state. We have reported the crystal structures of the polymorphs stable at ambient temperature for nematogenic *p*-azoxyanisole[6] and smectogenic ethyl *p*-azoxybenzoate.[7] The present paper reports an application of this rationale to the single smectic mesophases of three compounds. As an introduction, the various smectic polymorphs, their classification, and the kinds of information provided by different methods of investigation are next presented.

In the smectic mesophase, polymorphism has long been known because individual compounds sometimes exhibit several polymorphic forms, separated by first order transitions at definite temperatures.

Demus and Sackmann[8,9] initially characterized three of the polymorphs, primarily on the basis of complete mutual miscibility between polymorphs of the same type, but secondarily on the appearance of the phases as viewed with a polarizing microscope. Subsequent work in that laboratory increased the number of polymorphs to five,[1] and then to seven,[10] while deVries[11] has recently reported an eighth form. These forms are designated with the letters *A* through *H*, and an important problem is the determination of the molecular organization characteristic of each of these. Optical evidence concerning the molecular organization is generally scanty, and is totally lacking for polymorphs *E*–*H*.

Sackmann and Demus[1] propose that the smectic *D* form, which can be optically isotropic, may consist of spherical clusters packed in a cubic lattice. Taylor, Fergason and Arora[12] have found that oriented samples of forms *A*–*C* may be distinguished from their interference figures, the *A* form being uniaxial while the *B* and *C* polymorphs are biaxial. On this basis, and from the observation that the molecular lengths are in approximate agreement with the interlayer spacing (as determined by X-ray diffraction), it has been suggested[9,13] that the molecules in the smectic *A* form are approximately perpendicular to the molecular layers, and in the *C* modification are tilted at some fixed, but occasionally temperature-dependent,[14] angle with respect to the normal. This suggestion has received support from *X*-ray diffraction studies. Thus, de Vries[5] reports that the molecules of ethyl *p*-ethoxybenzal-*p*-aminobenzoate are approximately normal to the planes of the smectic *A* phase, while Chistyakov and co-workers have found the molecules to be tilted in the smectic *C* phases formed by the homologous series of dialkyl ethers of *p*-azoxyphenol from C_7 to C_{10},[15] and for *p*-nonyloxybenzoic acid.[16] On the other hand, a contrary example is provided by the smectic phase of thallium stearate investigated many years ago by Herrmann.[17] He found the smectic spacing to be longer than the molecular length but shorter than that of the head-to-head dimer, and concluded that the molecules are dimerized about the carboxyl groups and tilted 47° from the perpendicular to the smectic planes. Thallium stearate, perhaps the classical example of a tilted phase, was initially classified as a smectic *C* phase; however, its interference pattern is uniaxial,[18] which indicates that its smectic modification

is the *A* variety. The common morphology and optical nature of the three compounds will be used here as the basis for their common designation as smectic *A*; consideration of miscibility as a criterion is postponed until the discussion.

Further results from photographic X-ray diffraction studies are that unoriented samples of all polymorphs *A–H* show a series of sharp inner rings which represent different orders of the interlayer spacing. At larger angles one finds either a diffuse halo (smectic *A*, *C*, *D* and *F*), or one or more sharp rings (smectic *B*, *E*, *G* and *H*). From these results, and diffraction studies of oriented samples, it can be concluded that some modifications (e.g., *A* and *C*) have only one-dimensional order, some (such as smectic *B*) have two-dimensional order within each layer, while others exhibit at least a degree of three-dimensional regularity, for example smectic modifications *E*, *G* and *H*. While this kind of information is rather far removed from detailed molecular organization, it illustrates the existence of a variety of as yet undetermined molecular organizations in thermotropic mesophases. One might point out that a multitude of complex arrangements[19–22] have also been observed in lyotropic systems.

Information more closely approaching detailed molecular organization has been obtained by Chistyakov[23] and by Vainstein and Chistyakov,[24,25] who have studied smectic, nematic, and cholesteric phases by means of the cylindrical distribution function obtained through the Fourier transform of the photographically recorded diffraction patterns. These studies suggest possible modes of lateral packing of the molecules, but do not indicate the motif characteristic of each of the phases.

This survey demonstrates that there has been considerable progress in describing the macroscopic properties of mesophases, and a growing awareness of the diversity of polymorphic forms which these phases exhibit. On the other hand, a fundamental understanding is still lacking of the molecular arrangements characteristic of each of the various polymorphic forms and, still more, of the features of molecular structure which would enable one to predict the formation of a given mesomorphic polymorph. This paper is concerned with a quantitative X-ray diffraction study of the Bragg reflections from the smectic *A* polymorphs of three compounds in the form of well-oriented stepped drops, i.e., single liquid crystals. The data are

analyzed in two stages. In Sec. 3 the stepped drops are considered as mosaic scattering structures characterized by a " crystallite size " in the direction normal to the smectic layers, and subject to distortions of the first kind (the best known being thermal vibrations) and of the second kind (paracrystal distortions). As a result of that analysis, scattering amplitudes corrected for lattice imperfections are obtained which, in Sec. 4, we explain in terms of the one-dimensional projection of several centrosymmetric dimeric motifs comprising alternative partial descriptions of the molecular organization in these three smectic *A* mesophases. In Sec. 5, conclusions are drawn about the molecular organization.

2. Experimental

The three compounds investigated were bis(*p*-*n*-hexyloxyphenyl) mercury (BHPM),

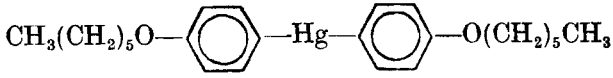

ethyl *p*-azoxybenzoate (EPAB),

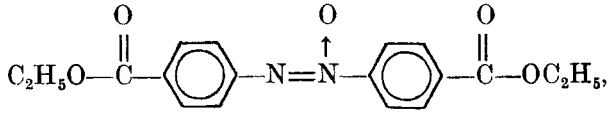

and thallium stearate (TLST),

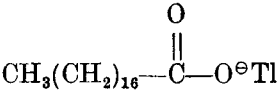

BHPM was prepared by decomposition of the double salt of *p*-*n*-hexyloxyphenyl diazonium chloride and mercuric chloride with copper, followed by treatment with NH_3, according to the method of Nesmejanow and Kahn.[26] Recrystallization from acetone yielded a product whose elemental analysis agreed well with that expected for $C_{24}H_{34}O_2Hg$. Details of the preparation and properties of several bis(*p*-*n*-alkyloxyphenyl)mercury homologues will be given in a forthcoming publication. EPAB was prepared by oxidizing ethyl *p*-azobenzoate, dissolved in glacial acetic acid at about 50 °C, with many small portions of 30% H_2O_2 over a period of several days until the initially orange–red solution became yellow. Addition of water

then precipitated EPAB, which was recrystallized from ethanol. The intermediate ethyl *p*-azobenzoate was prepared from ethyl *p*-aminobenzoate by the method of Meyer and Dahlem.[27] TLST was prepared by the procedure of Holde and Selim,[28] using a TlOH solution freshly prepared as the filtrate from the reaction of Tl_2SO_4 and $Ba(OH)_2$ solutions. TLST was recrystallized from hot ethanol. Table 1 shows the transition temperatures (°C) observed for these compounds using a Bausch and Lomb polarizing microscope equipped with a Kofler hot stage. The thermometer was calibrated over the temperature range 82–175° using three standards supplied with the hot stage, and the temperatures are believed to be accurate to ±0.5°. The ranges given in Table 1 indicate the temperatures at the beginning and end of the transformation.

TABLE 1 Phase Transformations of the Three Smectogenic Compounds.[a]

BHPM:	C ⇄ (118.7–119.9) I; C → (b) → S; I → 97.1–97.5 → S
EPAB:	C(I) ⇄ (101–103) C(II) ⇄ (115.6–115.8) S ⇄ (122.7–123.1) I
TLST:	C ⇄ (112.4–113.4) S ⇄ (174.7–175.1) I

(a) The phases are designated by the abbreviations C = crystalline, S = smectic, I = isotropic liquid.
(b) Crystallization of smectic BHPM occurs in the range 97–68°, with the smallest drops crystallizing spontaneously at 68 °C.

Microscopic examination of the three smectic phases under a cover slip in a polarizing microscope revealed for EPAB and BHPM the simple fan-shaped texture which Sackmann and Demus[9] have indicated is characteristic of the smectic *A* modification. The texture of TLST, usually homeotropic, could not be identified unambiguously as belonging to smectic *A* or *C*.

The supporting surfaces used to prepare the stepped drops for the diffraction experiments were flakes of glass or freshly cleaved mica

approximately 2 mm on a side and 4 μm thick. The flake bearing an appropriate amount of smectogenic material was heated on a microscope hot stage, either to the smectic temperature range (for TLST), or (for BHPM and EPAB) 10° past the isotropic transition temperature, and then rapidly cooled into the smectic temperature range. Drops which were approximately round and 200–600 μm in diameter were selected for further examination from those which were most

Figure 1. Photomicrograph of two types of smectic *A* stepped drops illustrated for EPAB on mica at 118 °C (45 ×).

nearly optically homogeneous when viewed between crossed polarizers. This served only for preliminary screening; the perfection of orientation could only be judged by diffractometer examination. Two types of stepped drops obtained are illustrated in the photomicrograph shown in Fig. 1. The lower specimen, a *large plateau* stepped drop, is characterized by a series of dark rings which clearly outline each plateau. Above this in the same photo is a *ringed* stepped drop,

in which the dark lines are replaced by many focal conic bubbles or spheres. BHPM did not form the *large plateau* stepped drops. The flake bearing a selected stepped drop, which had crystallized on cooling to room temperature, was mounted vertically in a small heated sample chamber. The sample chamber was fastened to a goniometer head, and its temperature was controlled to $\pm 0.5°$ by a thermistor and measured by a thermocouple. Upon heating, the sample regained the stepped drop texture.

The stepped drop samples were aligned by the procedures used for single crystals. The measurements were performed with CuK_α radiation, a scintillation counter, and pulse height analyzer. A graphite monochromator inserted in the diffracted beam significantly improved the peak-to-background ratio for these measurements. Sharp reflections were observed only along the reciprocal lattice direction normal to the smectic planes, and we will arbitrarily refer to this direction as c^* in reciprocal space, and as c in direct space. An ω scan, which involves only motion of the sample, was utilized to verify that the stepped drops were well oriented. The Bragg reflections have half-widths in ω varying from 0.05° to 0.16°, which are in the range of values typical of good single crystals. The peak shapes were carefully determined, integrated intensities were measured by the $\theta/2\theta$ scan technique (using a range of 2° in 2θ and a scan rate of 1°/min) and the background was counted for 40 sec on each side of the peak. The mean deviation of the intensities measured in repeated trials ranged from 0.35% for the stronger reflections to 8.3% for the weakest. The intensities decreased quite rapidly with order for all samples. We were able to measure six orders for TLST, and three for EPAB, but only the first order for the BHPM stepped drop. Hence, about 3 mm of isotropic BHPM was drawn into a section of 0.3 mm X-ray capillary, and the section mounted in the heated sample holder. On slow cooling from the isotropic to the monotropic smectic phase, homogeneously birefringent regions formed. One of these was placed in the X-ray beam. The half-width of the ω scan for this sample was 9.3°, indicating that it consists of a number of ordered regions differing somewhat in alignment. However, due to the much larger volume irradiated, it was possible to collect intensity data for two orders of BHPM using this sample. These intensities may not be as precise as those measured for other samples.

3. Parameters of the Paracrystal Model

The most characteristic feature of the meridional reflections observed for the three smectic A phases is the rapid decrease of the integrated intensity with order, as shown in Fig. 2. Less apparent is a progressive broadening of the line profile in 2θ with increasing

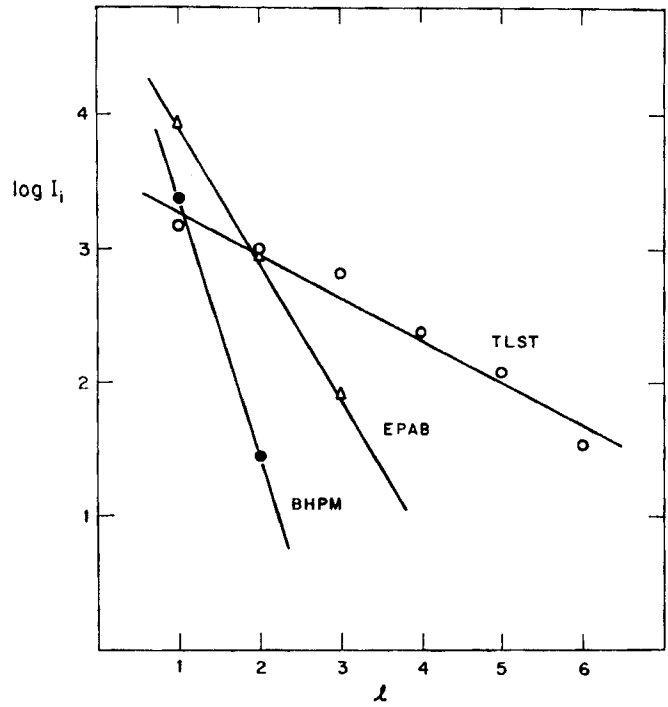

Figure 2. Variation of integrated intensity (logarithmic scale) of the meridional reflections with order for three smectic A phases.

order, shown quantitatively in Table 2 as an increase with order of the corrected integral line breadth β. The observed integral breadth, β_l, for the reflection of order l is defined as the ratio of the integrated to peak intensities (both corrected for background). Values of β are expressed in the units $Å^{-1}$. For this purpose the peak intensity is expressed in (counts/min) and the integral intensity is an integral of the intensity (in the same units) over the scan range

TABLE 2 Integral Line Breadths and Peak-to-Background Ratios for Three Smectic *A* Materials

Sample	l	$2\theta(°)$	Trial 1 $10^3\beta(Å^{-1})$	Trial 1 α	Trial 2 $10^3\beta(Å^{-1})$	Trial 2 α
BHPM/glass (93 °C)	1	3.17	2.66	4.16		
BHPM/mica (89 °C)	1	3.17	2.16	1.52		
BHPM/0.3 cap.	1	3.17	4.64	27.7		
(96 °C)	2	6.34	5.45	0.50		
EPAB/glass	1	4.33	2.76	20.5		
(116 °C)	2	8.66	2.52	2.66		
	3	13.00	4.37	0.12		
EPAB/mica	1	4.33	1.11	17.0	1.32	136
(116 °C)	2	8.66	a	a	a	a
	3	13.00	3.31	0.39	2.34	1.07
TLST/glass	1	2.32	2.11	9.38	2.07	7.32
(120 °C)	2	4.64	2.23	32.0	2.13	15.3
	3	6.96	2.42	21.2	2.50	11.3
	4	9.28	3.04	7.62	3.23	4.07
	5	11.61	3.90	3.28	5.27	2.08
	6	13.96	4.78	0.64	b	b
TLST/mica	1	2.32	2.17	8.03		
(121 °C)	2	4.64	2.41	33.6		
	3	6.96	2.50	27.4		
	4	9.28	a	a		
	5	11.61	3.50	4.17		
	6	13.96	6.12	0.97		

(a) Interference encountered with a reflection from the mica substrate.
(b) Unobserved.

in reciprocal lattice units, $2\sin\theta/\lambda$. These values are corrected for instrumental broadening β_x using the relation $\beta^2 = \beta_i^2 - \beta_x^2$, which assumes gaussian profiles. The value of β_x, 7.13×10^{-4} Å^{-1} was obtained from measurement of the (111) reflection of a 50 μm crystal of basic beryllium acetate. Also appearing in Table 2 are values of the ratio, α, of the integrated intensity I_i to the integrated background intensity I_b. The former is corrected for background, and the integration is performed over 2θ (degrees). For the latter, the average of the intensities (counts/min) measured 1° on each side of the peak are multiplied by the angular range equivalent to one reciprocal lattice spacing c^*.

The model which, in this section, we attempt to fit to the data of Table 2 is a one-dimensional mosaic paracrystal having distortions of the second kind, and hence being deficient to some degree in long-range order. Further, the paracrystal is assumed to be affected by distortions of the first kind (the best-known of which is thermal disorder), which do not cause loss of long-range order. The method of analysis[29] utilizes the facts that distortions of the first kind do not affect the integral breadth of the reflections, whereas the broadening effects of finite crystallite size and of distortions of the second kind are different functions of the order of the reflection—the former being independent of order while the latter increases with order. The integral breadths of two (or more) orders of reflection permit quantitative evaluation of the crystalline size and the extent of distortions of the second kind. Moreover, finite crystallite size does not contribute to the background intensity, whereas distortions of the first and seconds kinds cause a quantitative transfer of intensity from the diffraction peak to the background. Consequently values of α, coupled with a knowledge of the magnitude of distortions of the second kind, permit a quantitative evaluation of distortions of the first kind. The detailed analysis follows.

We designate the two contributions to the integral breadth β as $\beta_s = 1/L_c$ (due to the finite crystallite size L_c) and β_2 (from distortions of the second kind). If these components are assumed to be gaussian functions, there follows

$$\beta^2 = \beta_s^2 + \beta_2^2(l) \tag{1}$$

where the dependence of β_2 upon the diffraction order l has been explicitly indicated. From a knowledge of the component $\beta_2(l)$ of the integral breadth one may evaluate the order-independent paracrystal distortion factor g_2,

$$g_2 = (\overline{u_{2c}^2})^{1/2}/c \tag{2}$$

where c is the lattice spacing and $(\overline{u_{2c}^2})^{1/2}$ is the *rms* displacement along the c direction of the lattice sites of the paracrystal from the sites of a perfect lattice. The relation is [29]

$$\exp(-2\pi^2 g_2^2 l^2) = 1 - 2c\beta_2(l). \tag{3}$$

Upon substitution for $\beta_2(l)$ from Eq. (1) and solving for g_2, there is obtained

$$g_2 = \frac{0.342}{l}\,[-\log\{1 - 2c[\beta^2(l) - (1/L_c)^2]^{1/2}\}]^{1/2}. \tag{4}$$

If data are available for at least two orders, one may take advantage of the fact that g_2 and L_c are independent of l to solve this relation for g_2 and L_c using a proposed[29] iterative procedure. The resulting values for our smectic samples are entered in Table 3, together with the interlayer spacing c. Variances indicated for g_2 or L_c refer to differences for duplicate samples. For any given TLST sample, g_2 could be determined to higher precision, ± 0.0002, when the results from pairs of orders are compared.

TABLE 3 Distortion Parameters for the Smectic A Samples

Sample	g_2	L_c(Å)	c(Å)	g_1	B
BHPM/0.3 cap.	0.048	220[a]	27.9 ± 0.1	0.07	300
EPAB/glass	0.029	370		0.05 ± 0.02	55
			20.4 ± 0.1		
EPAB/mica	0.025 ± 0.003	860 ± 100		0.03 ± 0.01	15
TLST/glass	0.0250	480 ± 8		0.02 ± 0.01	45
	± 0.0009		38.1 ± 0.1		
TLST/mica	0.0215	440		0.02 ± 0.01	45

(a) The single order for BHPM on mica gives as an upper limit $L_c = 460$ Å.

The integrated intensity I_0^0 of the reflection of order l from a perfect lattice is reduced by the presence of distortions of the second kind to $I_0^0(1 - Z)$, where[29]

$$Z = \frac{1 - \exp(-2\pi^2 g_2^2 l^2)}{1 + \exp(-2\pi^2 g_2^2 l^2)} \tag{5}$$

and the intensity lost from the peak, $I_0^0 Z$, is transferred quantitatively to the background. Distortions of the first kind further reduce the integrated intensity to $I_i = I_0^0(1 - Z)D$ and transfer the difference, $I_0^0(1 - Z)(1 - D)$, to the background. The Debye factor D is related to the order-independent parameter g_1

$$g_1 = (\overline{u_{1c}^2})^{1/2}/c, \tag{6}$$

where $(\overline{u_{1c}^2})^{1/2}$ is the *rms* displacement from the paracrystal lattice

sites along the c direction due to distortions of the first kind. This relation is

$$D = \exp(-4\pi^2 g_1^2 l^2). \tag{7}$$

Thus the background intensity arising from distortions of both the first and second kinds is

$$I_b = I_0^0[1 - D(1 - Z)]. \tag{8}$$

The ratio α of the integrated intensity I_i to the background intensity I_b is

$$\alpha = D(1 - Z)/[1 - D(1 - Z)]. \tag{9}$$

Both I_i and I_b contain the Lorentz polarization factor Lp described in Sec. 4; however, for any order the ratio α, like the integral breadth β, is unaffected by the Lp correction. Solving Eq. (9) for D, substituting that expression into Eq. (7), and solving for g_1 leads to

$$g_1 = (2\pi l)^{-1}\left[\ln\left(\frac{1+\alpha}{\alpha}\right) + \ln(1 - Z)\right]^{1/2}. \tag{10}$$

For each reflection Z is calculated from Eq. (5) using the value of g_2 found in Table 3. Then Z, along with the α value from Table 2, are inserted in Eq. (10) to evaluate g_1. Since g_1 is a characteristic parameter of disorder within the structure, one should obtain the same value of g_1 for each order studied. For any given sample, however, these values showed considerable variation with order, with a mean error of ± 0.01 for TLST on glass or mica, or EPAB on mica, and ± 0.02 for EPAB on glass. On the other hand, the average g_1 values obtained for different stepped drops of the same material were in better agreement that would be expected from this variation with order (e.g., $g_1 = 0.017$ and 0.019 for two TLST stepped drops formed on glass). These average g_1 values are presented in Table 3. The last column in Table 3 lists the conventional temperature factor B, related to the tabulated g_1 values by

$$B = 8\pi^2 c^2 g_1^2, \tag{11}$$

assuming that all distortions of the first kind are of thermal origin.

Several interesting observations can be made concerning the parameters in Table 3. First, both g_1 and g_2 increase in the order TLST < EPAB < BHPM, indicating that BHPM is the most disordered of the three structures, as might have been anticipated from Fig. 2. Also, the stepped drops formed on mica appear to have a somewhat higher perfection, as indicated by the smaller g_1 and g_2 values for mica. Comparison with other partially ordered materials is instructive. Hosemann, Lemm and Wilke[30] have reported g_2 values for semicrystalline polymers at ambient temperature which range from 0.02 for polyethylene to 0.20 to polyacrylonitrile, and values for lead ranging from 0.041 at 325 °C to 0.126 at 550 °C. Our values for g_2 fall in the lower end of this range, indicating that distortions of the second kind make a surprisingly small contribution to the disorder in our fluid samples. A similar conclusion is reached from the L_c values appearing in column three. L_c may be interpreted as an average length over which diffraction from the specimen occurs coherently. As shown by Buchanan, McCullough and Miller,[31] the method of analysis we have used gives the weight-average L_c. For comparison, Hosemann, Lemm and Wilke[30] have obtained L_c values of 90–300 Å for polyethylene; and 12 Å to > 50 Å for lead at 550 °C and 325 °C, respectively, while Buchanan and Miller[32] have reported crystallite sizes normal to the chain direction for isotactic polystyrene which range from 130 to 275 Å, depending upon the draw ratio and annealing conditions. When one considers that we are dealing with fluid samples, the large L_c values in column three imply a surprisingly highly ordered structure. On the other hand, the *rms* displacements along c corresponding to the measured g_1 values are much larger than those obtained for other systems. These are $(\overline{u_{1c}^2})^{1/2} = 2.0$ Å for BHPM, 0.6 to 1.0 Å for EPAB and 0.8 Å for TLST. For comparison, the g_1 values reported[30] for polyethylene correspond to $(\overline{u_{1c}^2})^{1/2}$ in the range 0.048 to 0.078 Å, and for isotactic polystyrene[32] to 0.19 to 0.33 Å. Values rather similar to the latter are obtained for the *rms* fluctuations of the nearest-neighbor distance in isotropic liquids (carbon tetrachloride[33] 0.38 Å and liquid lead[34] 0.42 Å). We conclude that a significant amount of the disorder in these stepped drop samples arises from distortions of the first kind, and that these must include other types of disorder in addition to the normal Debye thermal motion.

4. Analysis of Structures

We are now in a position to obtain sets of observed structure amplitudes, $|F_0(l)|$, corrected for lattice imperfections. For this purpose, the best set of data was selected for each compound. This consisted of the data of BHPM in the capillary (comprising two orders), EPAB on mica (because higher intensities were found for stepped drops on mica than on glass) and TLST on glass (since data were collected from two stepped drop samples on glass, and these were averaged). The intensities, I_i, shown in column three of Table 4

TABLE 4 Lattice Distortion Corrections and Observed Structure Factors

	l	I_i	$1-Z$	I_0	D	I_0^0	$\|F_0\|$	$\|F_0^0\|$
BHPM	1	2351	0.977	2406	0.82	2930	49.0	54
(capillary)	2	25.8	0.909	28.4	0.46	40	5.3	6
EPAB/mica	1	8908	0.995	8949	0.98	9130	94.6	96
	2	966	0.982	984	0.92	1070	31.9	33
	3	78.0	0.959	81.4	0.87	95	9.0	10
TLST/glass	1	1458	0.994	1467	0.98	1500	38.3	39
(average)	2	933	0.977	955	0.92	1040	30.9	32
	3	650	0.948	686	0.87	790	26.2	28
	4	223	0.908	246	0.78	315	15.7	18
	5	105	0.857	123	0.67	185	11.1	14
	6	26.7	0.795	33.6	0.55	60	5.8	8

were obtained by dividing the measured integrated counts by the Lorentz polarization factor, Lp, which for our experimental arrangement is

$$Lp = \frac{1 + \cos^2 2\theta \cos^2 2\theta_m}{2 \sin 2\theta.} \tag{12}$$

Here θ_m is the Bragg angle, 13.10°, for the graphite monochromator located in the diffracted beam. Division of I_i by $(1-Z)$ yields intensities, I_0, corrected for the presence of distortions of the second kind, which are listed in column five. Further division by D (given in column six) produces intensities, designated I_0^0 and listed in column seven, characteristic of the lattice without distortions. Columns eight and nine give the structure amplitudes, $|F| = I^{1/2}$,

corresponding to I_0 and I_0^0, respectively. We observe that even after correction for distortions of the first and second kinds, the $|F_0^0(l)|$ values for all three compounds decrease monotonically with increasing order. In view of the rather large uncertainties in the experimental g_1 values, we have regarded D (which embodies the effects of distortions of the first kind) as a parameter to be adjusted during structure refinement. Hence, we have used the observed structure amplitudes in column eight, which are only corrected for distortions of the second kind:

$$|F_0(l)| = [I_i/(1 - Z)]^{1/2}. \tag{13}$$

If the phases were known, the projection of the electron density along z, $\rho(z)$, could be calculated using Fourier methods,

$$\rho(z) = \frac{1}{c} \sum_{l=1}^{N} F_0(l) \exp(-2\pi i l z/c), \tag{14}$$

where the sum is carried over all observed orders. The electron density function calculated in this way will be broadened by distortions of the first kind, and the resolution will be limited by the fact that N is quite small for our samples. Various approaches may be taken to solve the phase problem. We have chosen to postulate model structures which we believe to be reasonable, and which incorporate a limited number of parameters to be varied during refinement. Since all the postulated structures are centrosymmetric, the phase angles can only take the values 0 or π and the problem reduces to the determination of the sign of each $F_0(l)$. Structure factors (including the sign) may be calculated for any selected model structure using the relation

$$F_c(l) = 2 \sum_{j=1}^{M} f_j \cos(2\pi i l z_j/c) \exp(-2\pi^2 g_1^2 l^2) \tag{15}$$

where f_j is the scattering factor for atom j located, in projection, at position z_j, and the sum is carried over the M atoms in the molecule. We have used the self-consistent-field atomic scattering factors.[35] The final factor in Eq. (15) reduces the calculated structure factors to account for distortions of the first kind, so that their magnitudes may be comparable with the observed $F_0(l)$. A scale factor is applied to the latter so that the sum over all observed orders is the same for $|F_0(l)|$ and $|F_c(l)|$. Correctness of a proposed structure may be

judged by comparison of the magnitudes of $|F_0|$ and $|F_c|$. For this purpose we have used the reliability index, RP, defined as:[36]

$$RP = \left[\frac{\sum_{l=1}^{N} \{|F_0(l)| - |F_c(l)|\}^2}{\sum_{l=1}^{N} |F_0(l)|^2} \right]^{1/2}. \tag{16}$$

If a structure is found which gives a low value for RP, one may assume the signs of F_c are correct, and combine these with the observed structure amplitudes, $|F_0|$, to compute a projection of the electron density using Eq. (14). This may be compared with the projected electron density of the model, but one must discount the extraneous features in the calculated $\rho(z)$ arising from series termination effects. The effect of truncation errors, as well as the broadening due to distortions of the first kind, may be minimized by calculating the projected electron density difference, $\Delta\rho(z)$, between the real and model structures:

$$\Delta\rho(z) = \frac{1}{c} \sum_{l=1}^{N} [F_0(l) - F_c(l)] \exp(-2\pi i l z/c). \tag{17}$$

Atomic positions for the model structures were determined using a standard set of bond lengths and angles in conjunction with the available crystallographic data. The crystal structure of the low temperature form of ethyl *p*-azoxybenzoate is known,[7] while the nearest analogous structure for TLST is that of silver stearate,[37] and for BHPM is di-*p*-tolylmercury.[38] The proposed models must be compatible with the observed diffraction behavior, i.e., the smectic structure is layered and has a known interlayer spacing. Further, the layers must be capable of sliding past each other, in view of the finite viscosity of the smectic phase. The knowns are the repeat distance c and the measured structure amplitudes. In addition, we may impose the further condition that $I_0(l)$ for all unobserved orders shall be smaller than that of the last observed order.

We assume that the unit cell must repeat along the z-direction with a translation c, and that the molecules pack so as to leave no large voids. With these restrictions, refinement of the few variable parameters allowed for a *monomeric* motif did not furnish a reasonable fit to the observed structure factors. Hence, we turned to the

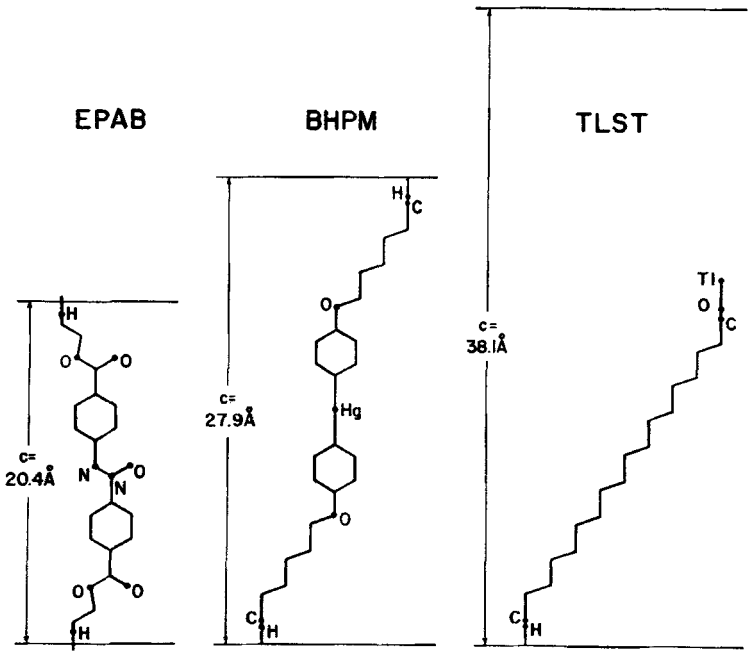

Figure 3. Molecular conformations assumed for trial structures of EPAB, BHPM and TLST.

next simplest motif—a *centrosymmetric dimer*. The particular motif chosen for BHPM is a centrosymmetric dimer composed of planar molecules having their alkyl chains in the *trans* zig-zag conformation, as illustrated in Fig. 3. The planes of the molecules in the dimer are parallel and separated by a distance A. The projection line of the molecule was taken along the C—Hg—C bonds, and the projection of the postulated molecular structure on this line gave a length, 27.9Å, in agreement with the observed interlayer spacing for this compound. When viewed edge-on, the planes of the molecules appear as a line segment of this length. The molecule of EPAB is nearly planar in the crystal, hence a planar dimer motif was chosen for this structure as well. As shown in Fig. 3, projection of the molecular length, including the van der Waals radius (1.20Å) of hydrogen, gave a length, 21.3Å, somewhat larger than the interlayer spacing found for the smectic A phase, 20.4Å. For both compounds the lateral separation A of the molecules was assigned the value 3.5Å, which is

approximately the distance of closest approach of the planes of the molecules allowed by the van der Waals radii.

For the first model examined the molecules were aligned parallel to the c direction (i.e., perpendicular to the smectic planes), and with no relative displacement along the c direction (Fig. 4a). Except for 4e, the planar molecules are viewed edge-on in Fig. 4. The first

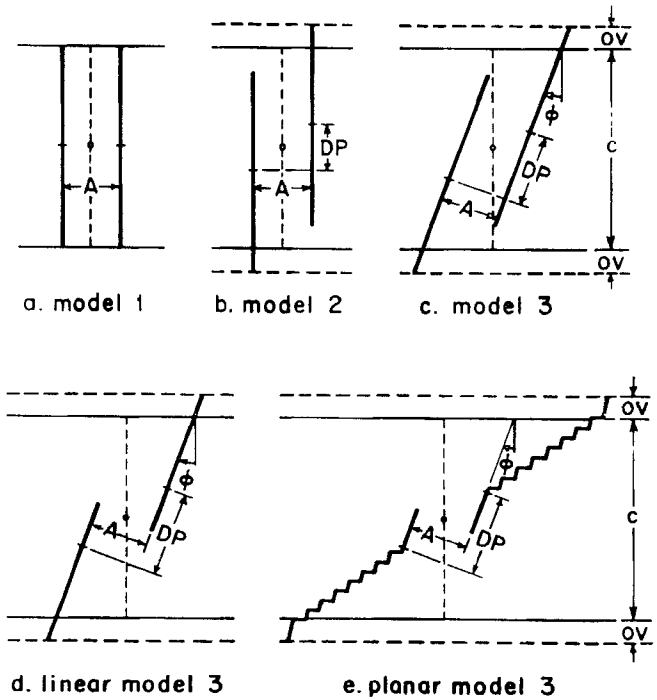

Figure 4. Schematic representation of the model structures for smectic phases. Parameters illustrated are the smectic layer spacing c, molecular overlap OV, molecular separation A, relative displacement DP of the two molecules, and angular rotation ϕ from the normal to the smectic planes.

model is a centrosymmetric analog of the accepted structure for the smectic A phase. In the absence of lattice imperfections, this model structure gives rise to large calculated intensities for some of the higher orders, and one attempts to obtain a reasonable fit to the observed structure amplitudes by varying the parameter g_1, which is the only adjustable parameter. Refinement of this model using data for two orders of BHPM produced as a minimum $RP = 0.5\%$

with $g_1 = 0.11$ ($B = 740$), and for three orders of EPAB on mica $RP = 1.43\%$ with $g_1 = 0.086$ ($B = 245$). These g_1 values are substantially larger than those appearing in Table 3, 0.07 and 0.03, respectively, which leads us to reject this model.

For the second model studied, the molecules were again maintained parallel to c but the molecules were displaced relative to each other by a distance, DP, along the c direction (Fig. 4b). Hence the molecules overlap the smectic planes by an amount $DP/2$. The displacement is measured from the points (indicated by the hash marks in Fig. 4) where a horizontal line through the center of inversion intersects the molecules in the position $\phi = 0$ and $DP = 0$. Refinement of these two parameters, DP and g_1, yielded a lower RP value for BHPM, 0.12%, with $DP = 5.50$ Å and $g_1 = 0.067$ ($B = 280$). This g_1 value is in quite satisfactory agreement with the corresponding entry, 0.07, found for BHPM in Table 3. However, the indicated overlap, 2.75 Å, is probably too large to permit the smectic layers to slip past one another. Hence despite the low RP value obtained for the second proposed model, we conclude that neither of these models furnishes a completely satisfactory representation of the smectic phase of BHPM. The fact that only two orders were observed restricts the number of variable parameters in any model to two; no other models were examined for BHPM. The second model likewise failed when applied to EPAB. In this case refinement produced a minimum in RP at $DP = 0$, thereby giving the same refined structure as obtained from the first model.

A third model was investigated for EPAB in which, in addition to the two degrees of freedom allowed in trial two, the molecules are permitted to tilt by an angle ϕ with respect to the normal to the smectic planes as shown in Fig. 4c. The extent of overlap is then determined by the values of A, DP and ϕ. This three parameter model produced a significant reduction of both RP and g_1 for EPAB. The best values of the parameters, $\phi = 29.7°$, $DP = 6.28$ (corresponding to an overlap of 0.97 Å), and $g_1 \geqslant 0.03$ ($B \geqslant 30$) reduced RP to 0.14%. The refinement was carried out by incrementing g_1 and then varying the other two parameters to minimize RP. We accepted the minimum g_1 which gave a low RP, although similar RP values could be obtained using larger g_1 values. This model furnishes a ten-fold improvement over the RP values obtained from the first

and second trial structures, and g_1 is now in satisfactory agreement with the value 0.03 ± 0.01 found in Table 3 for EPAB on mica. This tilt produces a gap of length 2.2 Å (measured along the molecule) between the molecules in adjacent layers. However, we believe that the structure obtained upon refinement of model three is the best representation of EPAB in the smectic state which can be deduced from the diffraction data.

TLST presents a more challenging problem for several reasons. If the alkyl chain is assumed to have the planar zig-zag conformation, the change in the molecular direction at the α-carbon atom makes two distinguishable dimer arrangements possible. It should be recalled that the length of the molecule is substantially less than the smectic interplanar spacing in this case, so that a dimeric motif is mandatory. Furthermore, for an alkyl chain of this length, the possibility should be investigated that one or more of the bonds may have the *gauche* conformation. We first consider two possible dimer arrangements, and will later return to the question of departures from the all-*trans* alkyl chain.

Let the alkyl chain define the plane of the molecule. If the carboxyl oxygen atoms lie in this plane, a sidewise pairing of molecules is indicated, with the two molecular planes parallel but displaced by the intermolecular separation. The centrosymmetric pair, with molecular planes seen edge on as shown in Fig. 4d, is termed the *linear dimer*. As before, the tilt angle ϕ is defined as that between the normal to the smectic plane and the molecular plane. This arrangement resembles that proposed for TLST in the smectic state by Herrmann,[17] except that we assume the —COOTl groups to overlap by analogy with the crystal structure of silver stearate.[37] A second possible arrangement arises if the carboxyl oxygens fall on a line perpendicular to the molecular plane, which allows a dimer to form with the two molecular planes coplanar. This is termed the *planar dimer* and is represented in Fig. 4e. If the tilt angle ϕ is defined as that between the smectic plane normal and the line formed by the α-carbon atom and Tl, the alkyl chain will be inclined to the normal by a larger angle, $\phi + 35.5°$, due to the bend at the α-carbon atom. These two dimers appear identical in projection when ϕ and the displacement DP are zero. The intermolecular spacing A was assigned the value 3.0 Å for both dimers.

A monomeric model is not possible for TLST since the molecule is shorter than the smectic spacing. Because the initial arrangement of the dimer pair corresponding to $DP = 0$ and $\phi = 0$ was arbitrary in this case, we began our analysis with the second model, involving relative displacement of the molecules and the temperature factor as adjustable parameters. The averaged data for TLST on glass, when applied to the linear dimer, refined to a minimum RP of 12.74% with $DP = 4.75$ Å and $g_1 = 0.021$ ($B = 50$). This result is unacceptable because both RP and the indicated overlap, 2.38 Å, are too large.

The third model used previously for EPAB, involving ϕ, DP and B as variables, led to an acceptable refinement of the linear dimer for TLST. The resulting parameter values were $RP = 1.73\%$ with $\phi = 25.1°$, $DP = 6.75$ Å, and $g_1 = 0.028$ ($B = 90$). This corresponds to a reasonable overlap, 0.73 Å. Equally good results were obtained with the three parameter planar dimer. In this case the minimum RP was found to be 1.74% with $\phi = 8.4°$, $DP = 5.98$ Å, and $g_1 = 0.028$ ($B = 90$). The overlap is 0.86 Å. This reasonably small value for the overlap for either model should impede, but not prevent, relative motion of adjacent smectic planes, in accord with the observed rather large viscosity. The low RP values found for these two dimer structures indicate quite good agreement between the calculated and observed structure amplitudes for the six orders. Further, the g_1 value, 0.028, obtained in each case stands in reasonable agreement with the value, 0.02 ± 0.01, found in Table 3 for TLST on glass. The structures resulting upon refinement of the two dimer models are nearly identical. The angle between the hydrocarbon chain and the normal to the smectic planes is 42.4° for the linear dimer and 43.9° for the planar dimer. These may be compared with the tilt angle of 47° reported for TLST by Herrmann.[17] The distance of separation of the thallium ions in projection along the c-axis is found to be 1.88 Å for the linear dimer and 1.86 Å for the planar dimer, suggesting strong coulombic interactions between the thallium and carboxylate ions, with a concomitant strong resistance to displacement of the layered structure. When viewed in projection, the linear and planar dimers differ only in the position of the carboxylate oxygens. This is presumably responsible for the slightly different values obtained upon refinement for the overlap, the angle between

the hydrocarbon chain and the smectic plane normal, and the separation of the thallium ions in projection.

Because our method determines only the best projection on the c-axis, equally acceptable models are generated by translation in the xy-plane of *one* molecule of the TLST dimer. If ϕ is non-zero, such an xy-translation can change both A and DP. An xy-translation at constant A is the major difference between the two TLST dimer models at refinement, and most of the difference between the two values for DP is thus explained. The rest results from the different locations of the carboxylate oxygens. For each type of dimer, the values of DP, A and ϕ at refinement determine which atomic groups of the dimer are in proximity. It is for this reason that a realistic value of A was selected. If A is altered, refinement will result in DP changing by an amount which depends on ϕ. However, for the linear model at refinement, reduction of A from 3.0 Å to 2.5 Å requires only a small reduction in DP from 6.75 Å to 6.51 Å, which allows the atomic groups involved in the intra-dimer contact to be determined with reasonable certainty. Changes which affect the projection on the c-axis markedly affect the value of RP. For example, near refinement, changes as small as 0.05 Å in DP change RP by 1–3% of its value; a change of 2–5 units in B has a similar effect.

It was found that the three models discussed above for TLST, as well as the two which will be considered below, all produced upon refinement the same set of phases for the first six orders, $- + - + - +$ (or $+ + + + + +$ if the origin is translated to the center of inversion at $c/2$).[39] This observation provides strong support for the correctness of our phase assignment. Hence, the observed structure amplitudes and the calculated phases produce the unique electron density for the TLST smectic phase shown in Fig. 5. Once the correctness of this profile is established, it provides a useful test of proposed structures. The intermeshed thallium and carboxylate ions give rise to the principal maximum in Fig. 5. The two subsidiary maxima on each side of the principal maximum are artifacts arising from series termination effects, as shown by examination of the electron density difference map and by the calculated electron density function for l through 10 using $F_c(l)$ deduced from the planar model. The region of low electron density represents the hydrocarbon tails. It is significant that the electron density distribution we have obtained

for six orders from thallium stearate shows no minimum near $z/c = 0$. Lesslauer, Cain and Blasie[40] have found a trough in the electron density (at the position of the terminal methyl groups) based upon six orders measured for three layers of hydrated magnesium stearate

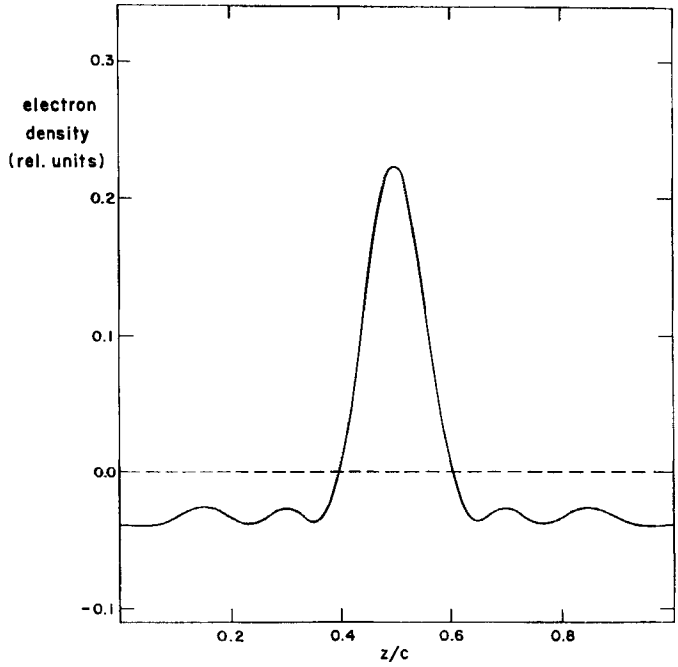

Figure 5. Electron density projection obtained using the structure amplitudes measured for TLST on glass and the calculated phases.

leaflets, and for only three diffraction orders from vesicles of dipalmitoyl lecithin/cardiolipin. A similar trough was obtained by Levine, Bailey and Wilkins[41] in their study of dipalmitoyl lecithin leaflets. Nerve myelin also exhibits a minimum electron density in the methyl region as illustrated, for example, by the 10 Å resolution structure recently reported by Caspar and Kirschner.[42] Evidently the molecules do not overlap significantly in the methyl region in these examples, whereas the overlap for thallium stearate is sufficient to produce a nearly uniform electron density across this boundary. This suggests that the hydrocarbon chains of TLST are fully extended, since an irregular interface created by extensive kinking of some of

the chains would inevitably lead to a large decrease in electron density in the methyl region.

The possibility has been suggested[43] that the long hydrocarbon chains of TLST might depart from the energetically favorable all-*trans* conformation. In order to investigate this, we have examined two conformers in which two bonds are rotated into the *gauche* position, thereby leaving the chain direction essentially unaltered. Using the nomenclature of Flory,[44] these differ in having bonds 4 and 6 (numbered from the methyl group) with either the conformation g^-, g^+ (kinked chain I) or g^+, g^- (kinked chain II). These conformers were inserted in the planar dimer arrangement. Refinement of the three parameters of the third model gave larger *RP* values than those obtained with the all-*trans* conformers in the linear or planar arrangement. Kinked chain I could be clearly excluded because of the large *RP* value, 6.4%, and the fact that the kink causes two of the methylene groups to overlap in projection, producing an unacceptable maximum in the calculated electron density difference function. Kinked chain II refined to a structure rather similar to that obtained for the linear and planar dimer structures. The indicated overlap, 0.82 Å, was nearly the same, and the separation of the thallium ions on projection is only 10% larger, 2.04 Å. While kinked chain II cannot be eliminated with certainty, the agreement between the calculated and observed structure amplitudes is clearly inferior to that obtained with the *trans* conformer in either dimer arrangement, as indicated by the larger *RP* value, 3.1%.

Pelzl and Sackmann[43] have studied the temperature dependence of the birefringence for an homologous series of thallium soaps. The higher homologues, including thallium stearate, exhibit a positive birefringence which decreases with temperature. They interpret this decrease as indicating a reduction of the interlayer spacing with temperature, which might arise from increased kinking or interpenetration of the hydrocarbon tails. Our study was performed at 120 °C, whereas their measurements covered the range 120–166 °C. Since the ratio of *gauche* to *trans* bonds will increase with temperature, our data cannot preclude the possibility that there is considerable kinking of the hydrocarbon chains at temperatures above 120 °C. On the other hand changes in the dimeric motif, such as an

increasing tilt angle ϕ, might offer an equally plausible explanation of their observations.

5. Discussion

Our most significant observation is that the intensities of the meridional reflections from all three smectic A phases, after correction for lattice imperfections, decrease rapidly and monotonically with order. In order to make optimum use of the known geometry of the molecules involved, we have chosen to interpret this decrease using models which are as realistic as possible, but which contain only a limited number of adjustable parameters. The first model, having the molecules arranged in layers with their long axes perpendicular to the smectic planes, most closely resembles the currently accepted description of smectic A phases. In this case the decrease of intensity with order must be ascribed entirely to distortions of the first kind. This model proved unsatisfactory for all three compounds investigated. It could not be applied to TLST, and for the other two compounds the g_1 (or B) values required to fit the intensity decrease with order were much larger than those measured. A second model, having as its motif a pair of molecules lying perpendicular to the smectic planes, but with the molecules displaced along this direction, was likewise rejected for BHPM and TLST because the molecules were required to overlap the smectic planes by an excessive amount to achieve agreement with the observed structure amplitudes, and RP was too large for TLST. Quite acceptable structure amplitudes were obtained for EPAB and TLST using a three parameter model allowing both displacement and tilting of the molecules with respect to the smectic plane normal.

Table 5 lists the parameters characterizing the best structures for the three smectic A phases upon refinement. The motif common to the EPAB and TLST models is a dimer having a displacement of 6–7 Å and sufficient tilt to reduce the overlap to less than 1 Å. This arrangement spreads the projected electron density more uniformly, and is primarily responsible for the observed monotonic decrease of the structure amplitudes with order. The fact that the observed variation of structure amplitudes with order could be represented by a dimeric motif, but not using a monomeric motif, does not prove

that the molecules actually exist as pairs within the smectic layer. Indeed, the cluster of molecules which moves coherently might be considerably larger as suggested, for example, by the model of the smectic state proposed by de Gennes.[45] Whatever the cluster size

TABLE 5 Parameters of the Best Structures Obtained Upon Refinement

	BHPM	EPAB/mica	TLST/glass (linear)	TLST/glass (planar)
RP (%)	0.12	0.14	1.73	1.74
displacement (Å)	5.50	6.28	6.75	5.98
overlap (Å)	2.75	0.97	0.73	0.86
molecule tilt (°)	—	29.7	42.4	43.9
g_1	0.067	0.030	0.028	0.028
B (Å^2)	280	30	90	90

may be, our results carry the implication that lateral attractions between molecules are of importance for the formation of a smectic *A* phase. Some evidence for strong lateral attractions is found in the molecular packing of these compounds in the crystalline state. If silver stearate is accepted as an analog of TLST, the intermeshed silver and carboxylate ions proposed for this structure[37] provide evidence for very strong attractions, as mentioned above. The crystal structure of EPAB[24] revealed that the azoxy and carbonyl groups are all *cis* to each other, which was unexpected. This results in a large dipole moment directed in the plane of the molecule, and transverse to its long axis. Further, the dipolar interactions are all attractive along the distance of closest approach of molecules in the crystal, which implies that these interactions are a significant factor in determining the molecular packing in the crystalline state. The crystal structure of di-*p*-tolylmercury[38] suggests the possibility of weak attractions between the mercury and the pi cloud of the aromatic ring of the adjacent molecule.

Of the three compounds examined, one—EPAB—exhibits a smectic *A* phase as judged by all criteria.[8] The morphology of smectic BHPM formed on cooling the isotropic liquid—a focal-conic (fan-shaped) texture arising from the coalescence of batonets—optically typifies smectic *A* phases. The third compound, TLST, is one of the thallium salts reported[43] to form this texture under the same

conditions. Further, it is reported[18] to be optically uniaxial, as are the other smectic *A* phases. Baum, Demus and Sackmann,[46] however, have found that these smectic (neat phase) thallium salts are *not* completely miscible over the entire composition range with either the sample smectic *A* or smectic *C* phases which they examined. Therefore, despite the morphological resemblance of smectic TLST to smectic *A* phases, and its uniaxial nature, it cannot be classified as smectic *A* if one insists upon the criterion of complete miscibility. As an indication of molecular organization, this criterion may be too restrictive, for the same authors[46] report that *isotropic* liquid phases of the thallium salts were not completely miscible with most—but not all—of the sample mesophasogenic compounds. Regardless of the label to be attached to smectic TLST, our results indicate that it and smectic *A* EPAB share the common feature of molecular tilt within one smectic layer. This feature could be compatible with the observed uniaxial optical property if the direction of tilt varied randomly throughout the sample thickness. Thus the smectic *A* and *C* forms must be distinguished on the basis of some property other than tilt within any one layer.

It should be mentioned that the question of molecular tilt within the smectic layers has also been studied by EPR using spin labels. Here it is assumed that the probe molecules execute rapid motion in a potential field which has its axis along the director of the host molecules. This involves the further tacit assumption that the organization of the host molecules in the immediate vicinity of the probe is not significantly perturbed by the presence of the probe. The orientation of the host molecules is not directly measured, but is inferred from the angular dependence of the hyperfine splitting when the sample is tilted with respect to the magnetic field. The observed angular dependence is compared with a theoretical prediction based upon an assumed preferred orientation of the director of the smectic molecules in the sample reference frame. For the smectic *C* phase of terephthal-*bis*-(4-*n*-butylaniline) Luckhurst and Sundholm[47] assumed the temperature dependent tilt angles measured optically for this phase by Taylor, Arora and Fergason,[14] and achieved good agreement with the temperature dependence of the hyperfine splitting measured at a single angle. Luckhurst and coworkers have reported that the molecules are perpendicular to the

smectic layers for the smectic *A* modification of this compound,[47] for the smectic *C* phase of 4, 4′-di-*n*-heptyloxyazoxybenzene,[48] and for the smectic *A* phase of EPAB.[49] Their conclusion concerning the smectic *A* phase of EPAB is in disagreement with that reached in this paper. It should also be noted that their spin label measurements for 4, 4′-di-*n*-heptyloxyazoxybenzene were interpreted as explicitly eliminating the possibility of molecular tilt, which conflicts with the results of diffraction study of this smectic *C* phase by Chistyakov and Chaikowsky.[15]

Turning to lattice imperfections in these smectic *A* phases, our study has revealed that between 12 and 42 smectic layers scatter coherently in oriented stepped drops, and that even in the more poorly oriented sample of BHPM in a capillary 8 layers scatter coherently. Further, distortions of the second kind make a surprisingly small contribution to the lattice disorder in these samples, while the *rms* displacements arising from distortions of the first kind are probably too large to be attributed to Debye thermal vibrations. For example, the g_1 value, 0.07, given for BHPM in Table 3 corresponds to an *rms* displacement of nearly 2 Å. De Gennes[45] has proposed a phenomenological model of the smectic state which may offer an explanation for the large g_1 values we have observed. He invokes longitudinal waves, which displace the molecules perpendicular to the layers, accompanied by transverse dilatation waves. In contrast to the general background of scattering predicted for independently vibrating particles by the Debye treatment of the temperature factor, the highly coupled motions involved in de Gennes' model will result in thermal diffuse scattering which is concentrated near the nodes of the reciprocal lattice. The background in our 2θ scans is fairly uniform between reflections, but this appearance may arise from overlap of the thermal diffuse scattering regions due to the small separation of the reciprocal lattice points.

REFERENCES

1. Chistyakov, I. G., *Sov. Phys.-Uspekhi* **9**, 551 (1967) [*Usp. Fiz. Nauk* **89**, 563 (1966)]; Saupe, A., *Angew. Chem. Internat. Edit.* **7**, 97 (1968); Sackmann, H. and Demus, D., *Fortschr. Chem. Forsch.* **12, 349 (1969).**
2. Delord, P. and Falgueirettes, J., *Compt. rend.* **260**, 2468 (1965).
3. deVries, A., *Acta Cryst.* **A25**, S135 (1969).

4. deVries, A., *Mol. Cryst. and Liq. Cryst.* **10**, 31, 219 (1970).
5. deVries, A., *ibid.* **11**, 361 (1970).
6. Krigbaum, W. R., Chatani, Y. and Barber, P. G., *Acta Cryst.* **B26**, 97 (1970).
7. Krigbaum, W. R. and Barber, P. G., *ibid.* **B27**, 1884 (1971).
8. Demus, D. and Sackmann, H., *Z. phys. Chem.* (Leipzig) **222**, 127 (1963).
9. Sackmann, H. and Demus, D., *Mol. Cryst.* **2**, 81 (1966).
10. Demus, D., Diele, S., Klapperstück, M., Link, V. and Zaschke, H., *Mol. Cryst. and Liq. Cryst.* **15**, 161 (1971).
11. deVries, A., *ibid.* **16**, 311 (1972).
12. Taylor, T., Fergason, J. L. and Arora, S., *Phys. Rev. Letters* **24**, 359 (1970).
13. Saupe, A., *Mol. Cryst. and Liq. Cryst.* **7**, 59 (1969).
14. Taylor, T. R., Arora, S. L. and Fergason, J. L., *Phys. Rev. Letters* **25**, 722 (1970).
15. Chistyakov, I. G. and Chaikowsky, W. M., *Mol. Cryst. and Liq. Cryst.* **7**, 269 (1969).
16. Chistyakov, I. G., Schabischev, L. S., Jarenov, R. I. and Gusakova, L. A., *ibid.* **7**, 279 (1969).
17. Herrmann, K., *Trans. Faraday Soc.* **29**, 972 (1933).
18. Fergason, J. L., private communication.
19. A survey of the extensive work of V. Luzzati and co-workers may be found in Chapter 3 of D. Chapman, ed., *Biological Membranes*, Academic Press, London (1968).
20. Lawrence, A. S. C., *Mol. Cryst. and Liq. Cryst.* **7**, 1 (1969).
21. Balmbra, R. R., Clunie, J. S. and Goodman, J. F., *ibid.* **3**, 281 (1967).
22. Lawson, K. D., Mabis, A. J. and Flautt, T. J., *J. Phys. Chem.* **72**, 2058 (1968).
23. Chistyakov, I. G., *Sov. Phys.-Cryst.* **8**, 691 (1964).
24. Vainshtein, B. K. and Chistyakov, I. G., *Sov. Phys.-Doklady* **8**, 1044 (1964).
25. Vainshtein, B. K. and Chistyakov, I. B., *Growth of Crystals* **5A**, 133 (1968).
26. Nesmejanow, A. and Kahn, E., *Ber. dtsch. chem. Ges.* **62B**, 1018 (1929).
27. Meyer, A. and Dahlem, K., *Justus Liebigs Ann. Chem.* **326**, 331 (1903).
28. Holde, D. and Selim, M., *Ber. dtsch. chem. Ges.* **58A**, 523 (1925).
29. Bonart, R., Hosemann, R. and McCullough, R., *Polymer* **4**, 199 (1963).
30. Hosemann, R., Lemm, K. and Wilke, W., *Mol. Cryst.* **2**, 333 (1967).
31. Buchanan, D. R., McCullough, R. L. and Miller, R. L., *Acta Cryst.* **20**, 922 (1966).
32. Buchanan, D. R. and Miller, R. L., *J. Appl. Phys.* **37**, 4003 (1966).
33. Narten, A. H., Danford, M. D. and Levy, H. A., *J. Chem. Phys.* **46**, 4875 (1967).
34. Kaplow, R., Strong, S. and Averbach, B., *Phys. Rev.* **138**, A1336 (1965).
35. *International Tables for X-Ray Crystallography*, Vol. III, Kynoch Press, Birmingham, England (1962).
36. Hamilton, W. C., *Acta Cryst.* **18**, 502 (1965).
37. Vand, V., Aitken, A. and Campbell, R. K., *Acta Cryst.* **2**, 398 (1949).
38. Mathew, M. and Kunchur, N. R., *Can. J. Chem.* **48**, 429 (1970).
39. Hybl, A., *Biophys. J.* **10**, 1121 (1970).
40. Lesslauer, W., Cain, J. and Blasie, J. K., *Biochim. Biophys. Acta* **241**, 547 (1971).
41. Levine, Y. K., Bailey, A. I. and Wilkins, M. H. F., *Nature* **220**, 577 (1968).
42. Caspar, D. L. D. and Kirschner, D. A., *Nature New Biology* **231**, 46 (1971).

43. Pelzl, G. and Sackmann, H., *Mol. Cryst. and Liq. Cryst.* **15,** 75 (1971).
44. Flory, P. J., *Statistical Mechanics of Chain Molecules*, p. 56, Interscience, N.Y. (1969).
45. de Gennes, P. G., *J. Phys.* (Paris) *Suppl.* **30** C4, 65 (1969).
46. Baum, E., Demus, D. and Sackmann, H., *Wiss. Z. Univ. Halle* **XIX M,** 37 (1970).
47. Luckhurst, G. R. and Sundholm, F., *Mol. Phys.* **21,** 349 (1971).
48. Francis, P. D. and Luckhurst, G. R., *Chem. Phys. Letters* **3,** 213 (1969).
49. Luckhurst, G. R. and Sanson, A., *Mol. Cryst. and Liq. Cryst.* **16,** 179 (1972).